

Effect of Pyrolysis Temperature on the Leaching Behaviour of Spent Lithium Iron Phosphate Batteries with Sulfuric Acid and Sodium Hydroxide Solution

Kezya Sagita Indah Sari¹, Gideon Pambudi Laksono¹, Taufiq Hidayat¹, Zela Tanlega Ichlas^{1,*}, Bentang Arief Budiman^{2,3}, Arifa Sura Sembiring⁴, and Mohammad Zaki Mubarak¹

¹Department of Metallurgical Engineering, Institut Teknologi Bandung, Indonesia 40132

²Department of Mechanical Engineering, Institut Teknologi Bandung, Indonesia 40132

³National Center for Sustainable Transportation Technology, Institut Teknologi Bandung, Indonesia 40132

⁴Mineral Research Institute, Gotion High-Tech Indonesia, Indonesia 12950

Abstract. Greenhouse gas emissions from fossil fuel combustion account for approximately 68% of total global emissions, making their reduction essential to mitigating global climate change and achieving Net Zero Emissions by 2050. The transition to electric vehicles has accelerated the demand for lithium-ion batteries, particularly lithium iron phosphate (LFP) types, which are favoured for their reduced dependence to nickel and cobalt. This study explores the recycling of cylindrical spent LFP batteries through a processing involving seawater discharging, pyrolysis at 400–700 °C for 120 minutes, mechanical shredding, particle sieving, and leaching using 2.5 M H₂SO₄ and 5 M NaOH. Samples were characterized using scanning electron microscopy with energy-dispersive X-ray spectroscopy (SEM-EDS), X-ray diffraction (XRD), atomic absorption spectroscopy (AAS), and LECO carbon analyser. Pyrolysis at 500 °C produced the highest lithium content in the -45 mesh fraction, reaching 4.11 wt%, and resulted in optimal lithium recovery in the leachate, with 4561.51 mg Li per cell using H₂SO₄ and 1719.32 mg Li per cell using NaOH. Although H₂SO₄ achieved higher lithium extraction, NaOH demonstrated greater selectivity against iron. These findings indicate that 500 °C is an effective pyrolysis temperature for enhancing lithium recovery from spent LFP battery.

1 Introduction

CO₂ emissions from fossil fuel combustion contribute approximately 68% of total global greenhouse gas emissions. In 2023, global emissions reached 57.1 GtCO₂e, showing an increase of 1.3 percent compared to the previous year [1]. This makes CO₂ emissions the main contributor to global warming and climate change. Reducing global CO₂ emissions is essential to limit the average temperature rise to 1.5 °C and to reach Net Zero Emissions (NZE) by 2050 [1,2]. Electrification is one of the key strategies to achieve this target. The transition to electric vehicles is expected to account for 60 percent of total passenger car sales by 2030 [2]. A major portion of the total cost of an electric vehicle comes from its energy storage system, the lithium-ion battery (LIB) [3]. LIB play a critical role in decarbonization strategies to achieve the NZE scenario.

The production cost of LIB is largely driven by the cathode component, as the cathode represents the largest weight fraction in LIB and plays a key role in determining battery performance such as energy density, safety, and lifespan [4]. Commonly used cathode materials in LIB include lithium cobalt oxide (LCO), lithium manganese oxide (LMO), lithium iron

phosphate (LFP), lithium nickel manganese cobalt oxide (NMC), and lithium nickel cobalt aluminium oxide (NCA) [4,5]. The EV battery market is primarily dominated by LIB with NMC, NCA, and LFP [6].

End-of-life LFP-type LIB contains valuable materials such as cathode active material (CAM) from LiFePO₄, anode active material (AAM) from graphite, copper foil, aluminium foil, and battery casing made of steel and aluminium. Among these, CAM is the most valuable component, accounting for 30–40% of the total weight of an LFP battery [7]. Lithium is the most valuable element within CAM and is classified as a critical mineral due to its supply risk [7,8]. The lithium content in spent LFP batteries is higher than in primary mineral sources, making LFP battery recycling highly promising for extending the global lithium supply chain and reducing the risk of primary resource depletion [7]. Moreover, LFP battery waste contains hazardous substances that can pollute the environment and pose risks to human health. Therefore, recycling spent LFP batteries is a key solution to prevent pollution and support environmental sustainability [7].

This study systematically investigates the influence of pyrolysis temperature on the physicochemical characteristics of pyrolyzed products and examines how

* Corresponding author: zela@itb.ac.id

variations in both pyrolysis temperature and leaching media affect lithium recovery during subsequent leaching. The experimental program encompasses detailed characterization of phase evolution and product properties resulting from pyrolysis at different temperatures, quantification of the extent of material dissolution during leaching, and comprehensive analysis of the leaching residues. Through this approach, the work aims to elucidate the relationship between thermal pretreatment conditions and downstream leaching performance, providing insights for optimizing integrated pyrolysis–leaching routes for lithium recovery.

2 Experimental

The battery samples used in this study were cylindrical LFP 32140 cells supplied by PT Gotion High-Tech Indonesia, with a nominal voltage of approximately 3.2 V. Each cell measured approximately 13 cm in length and 3.25 cm in diameter. The leaching agents, namely H_2SO_4 and NaOH , were prepared from analytical-reagent-grade chemicals diluted with distilled water. The experimental work commenced with a controlled discharging step in seawater, followed by initial material characterization. Deactivated cells were cross-sectioned and examined using scanning electron microscopy coupled with energy-dispersive spectroscopy (SEM-EDS) to investigate their internal structure and elemental distribution. In parallel, additional LFP cells were mechanically shredded and sieved, and the resulting fractions were characterized using atomic absorption spectroscopy (AAS) for elemental quantification, X-ray diffraction (XRD) for phase identification, and carbon analysis to determine residual carbon content.

2.1 Initial characterization

The deactivated batteries were mechanically shredded using a battery-specific shredding machine. The shredded material was then sieved into size fractions of +18 mesh, -18 to +45 mesh, -45 to +100 mesh, -100 to +200 mesh, and -200 mesh using an electric sieve shaker. Sieving was carried out to separate casing and current collector fragments from finer electrode active materials. The -45 to +200 mesh fraction contains the highest lithium and iron content with minimal contamination from casing and foil, indicating that it mainly consists of CAM [9]. Accordingly, this particle size range was selected as the primary leaching feed. In this study, the -200 mesh fraction was also included as leaching feed to recover residual metals.

2.2 Pre-treatment process

The pre-treatment process began with pyrolysis, followed by mechanical shredding and sieving. During pyrolysis, intact and deactivated battery cells were placed in stainless steel crucibles, inserted into alumina tubes, and positioned in the hot zone of a horizontal tube furnace (HTF). The tubes were sealed to maintain an

inert atmosphere, and argon gas was flowed at 1 L/min. The samples were heated from room temperature to target pyrolysis temperatures with a 120-minute holding time, then cooled before removal. After pyrolysis, the batteries were shredded using a mechanical shredder set to 50 rpm, and the resulting material was sieved to isolate the electrode active material, particularly the fraction passing through 45 mesh.

2.3 Leaching process

For sulfuric acid leaching, 200 mL of 2.5 M H_2SO_4 solution was added to a 500 mL three-neck flask at a solid-to-liquid ratio (S/L) of 50 g/L. The flask was placed on a hot plate and equipped with a thermometer and a water-cooled condenser to maintain stable leaching conditions. For sodium hydroxide leaching, 5 M NaOH solution was used in a 500 mL PTFE reactor under the same S/L. The reactor was covered, and the temperature was monitored manually. After setup, both solutions were heated to a stable temperature of 60 °C. 10 grams of -45 mesh electrode active material, both untreated and pyrolysed at 400–700 °C, were separately introduced into the reactors. Leaching with sulfuric acid was stirred at 300 rpm, while sodium hydroxide leaching was stirred at 500 rpm. Notably, the use of different stirring rates was necessitated by differences in slurry behaviour under the respective leaching conditions. Each leaching process lasted 120 min. Subsequently, the leachate and residue were separated using vacuum filtration. The leachate was diluted to 500 mL using 3% HNO_3 (~0.5 M) for acid liquor and 5.2 M HNO_3 for alkaline liquor before AAS analysis. The residues were dried at 110 °C for approximately 12 h and stored. Selected residue samples were characterised by XRD, while others were digested and diluted to 100 mL with 3% HNO_3 for AAS.

3 Results and discussion

3.1 Changes in the internal structure of the battery during pyrolysis

The cathode region consists of aluminium current collector foil and LiFePO_4 (LFP) active material, while the anode consists of copper foil and graphite. Pyrolysis caused physical changes in both electrode regions. As shown in Figure 1, cross-sectional SEM images reveal that the polymer-based separator between the electrodes disappeared, likely due to shrinkage and melting at 135–165 °C [10]. At 400 and 500 °C, electrode structures remained largely intact. At 600 °C, small gaps began to form between the anode and cathode, likely due to the release of gases from the decomposition of the separator, electrolyte, and PVDF binder. At 700 °C, aluminium foil melted and oxidized into Al_2O_3 , visible as enlarged molten clusters in the cathode area. This oxidation may have occurred during furnace cooling, when residual oxygen from gas impurities or ambient air reacted with exposed battery components.

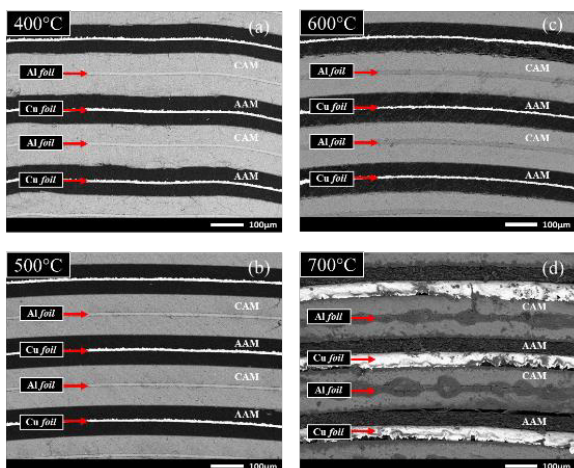


Fig. 1. Cross-sectional structure of LFP battery samples after pyrolysis at holding temperatures of (a) 400 °C, (b) 500 °C, (c) 600 °C, and (d) 700 °C.

3.2 Characteristics of pyrolyzed electrode active material

The XRD results of the -45 mesh electrode active material at various pyrolysis temperatures are shown in Figure 2. The detected phases include LiFePO_4 as the CAM and graphite as AAM. No metallic phases were observed, indicating that no carbothermic or aluminothermic reduction occurred during pyrolysis. Across all temperatures, the LiFePO_4 and graphite phases remained stable. Compared to the untreated sample, the LiFePO_4 peaks in pyrolysed samples appeared more intense, suggesting enhanced liberation of CAM from the aluminium foil during pyrolysis.

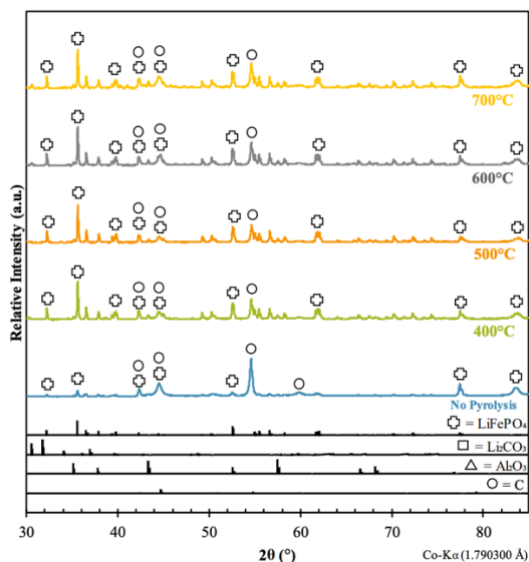


Fig. 2. XRD Analysis of -45 mesh electrode active material after pyrolysis at various temperatures

3.3 Composition of pyrolyzed electrode active material

Figure 3 shows the effect of pyrolysis temperature on the recovery of -45 mesh electrode active material per battery cell. Increasing the temperature from 400 to 600

°C led to higher recovery, reaching a maximum of 112.5 g per cell at 600 °C. At 400 °C, PVDF binder was only partially decomposed [11], resulting in lower recovery due to poor separation from the current collector. At 700 °C, recovery decreased to 91.7 g per cell, likely due to aluminium foil melting and capturing cathode material, which hindered its release. Without pyrolysis, recovery was significantly lower at only 28.8 g per cell, indicating the importance of pyrolysis for effective material liberation.

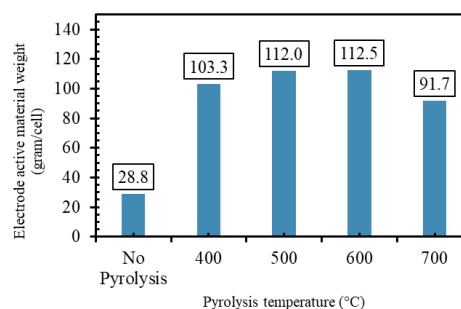


Fig. 3. Effect of pyrolysis temperature on the recovery of -45 mesh electrode active material after shredding and sieving

Figure 4 shows the composition changes of electrode active material after pyrolysis at 400–700 °C for 120 min. The main elements present were Li and Fe from the CAM, and C from the AAM. The non-pyrolysed sample had the highest C content (74.05%) but the lowest Li and Fe content, indicating poor separation of CAM from the aluminium foil. Li content increased with temperature up to 500 °C then slightly decreased at 700 °C. In general, pyrolysed samples had higher Li content than non-pyrolysed ones due to improved liberation of LiFePO_4 . Fe content slightly decreased with higher pyrolysis temperature. C content declined from 400 to 600 °C but increased again at 700 °C. Al and Cu levels remained low and relatively constant, confirming effective separation from foil fragments and better homogeneity as leaching feed. Li extraction in this study refers to the amount of Li dissolved in the leachate relative to its total content in the -45 mesh electrode active material per battery cell.

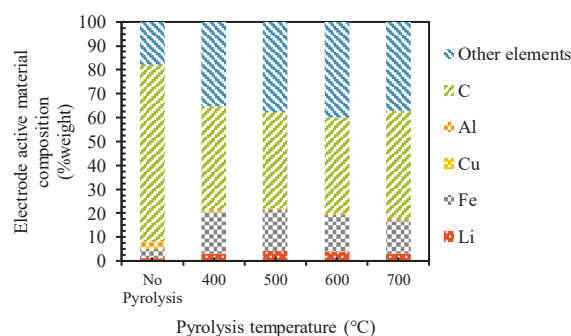


Fig. 4. Effect of pyrolysis temperature on the composition of -45 mesh electrode active material after shredding and sieving

3.4 Solubility of electrode active material in the leaching process

Figure 5 shows the amount of Li and Fe dissolved in sulfuric acid leaching, along with the percentage extraction for each pyrolysis temperature variation of the electrode active material. Lithium dissolution increased from 400 to 500 °C, but decreased from 600 to 700 °C. The highest Li recovery, 4561.51 mg Li/cell, was obtained from material pyrolysed at 500 °C. A similar trend was observed for Fe dissolution, with the highest recovery of 23349.09 mg Fe/cell at 500 °C. The lowest Li and Fe recovery observed from non-pyrolysed material.

Li extraction was highest in no-pyrolysed material at 99.78%, while the lowest was at 700 °C pyrolysis with 95.75%. Li extraction percentages at 400, 500, and 600 °C were 98.37%, 99.39%, and 97.17%, respectively. Highest Fe extraction was obtained in the 600 °C pyrolysis at 99.53%, with the lowest at 700 °C pyrolysis at 98.24%. For non-pyrolysed electrode active materials and those treated at 400 and 500 °C, the Fe extraction percentages were 99.36%, 99.02%, and 99.20%, respectively. These differences in extraction percentage reflect the varying ease of Li and Fe dissolution during leaching, influenced by the initial elemental concentrations in the electrode material.

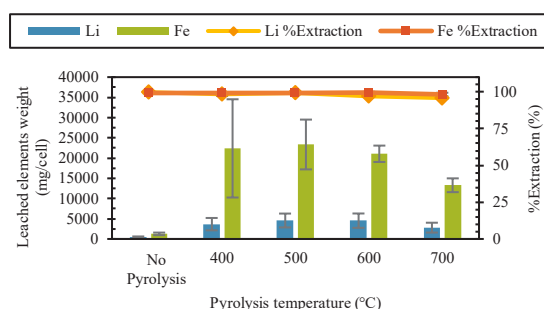


Fig. 5. Lithium and iron content and the percentage extraction of lithium and iron from the leaching process of pyrolyzed electrode active material using sulfuric acid as leaching media

Figure 6 shows the weight of Li and Fe dissolved and the percentage extraction of Li and Fe from the leaching process of pyrolysed electrode active material using sodium hydroxide as the leaching media. Li dissolution increased with pyrolysis temperature from 400 to 500 °C but decreased from 600 to 700 °C. The highest Li recovery, 1719.32 mg Li/cell, was obtained from material pyrolysed at 500 °C. Fe dissolution remained very low across all pyrolysis temperature variations. The highest Li extraction was obtained in the non-pyrolysed material at 84.05%, while the lowest was obtained in the 600 °C pyrolysed material at 38.36%. Li extraction percentages at 400, 500, and 700 °C were 39.86%, 45.74%, and 42.21%, respectively.

Fe extraction remained close to 0% at all pyrolysis temperatures, with the highest extraction in the non-pyrolysed material at 0.2%. At 400, 500, 600 °C, and 700 °C, Fe extraction percentages were 0.08%, 0.02%, 0.03%, and 0.02%, respectively. The low Fe content and

extraction percentages demonstrate the selectivity of sodium hydroxide in dissolving Li while separating it from Fe.

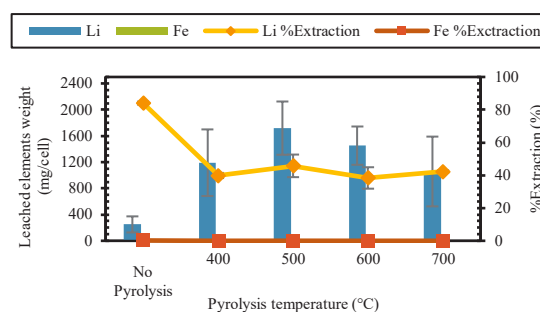


Fig. 6. Lithium and iron content and the percentage extraction of lithium and iron from the leaching process of pyrolyzed electrode active material using sodium hydroxide as leaching media

Similar to sulfuric acid leaching, the high Li extraction in the non-pyrolysed material indicates that Li is more easily dissolved in sodium hydroxide, even though in much smaller quantities, due to the low initial Li content in the untreated -45 mesh fraction. However, the amount of Li dissolved in sodium hydroxide was lower compared to sulfuric acid. The lower lithium extraction in the pyrolysed samples suggests that Li is more difficult to dissolve in sodium hydroxide, likely due to the constant leaching temperature of 60 °C. According to Yang et al. [12], Li extraction decreased significantly when leaching temperature increased from 50 to 60 °C due to the activation and collision of Li^+ and PO_4^{3-} ions, which form precipitates of Li_3PO_4 .

3.5 Characteristics and composition of leaching residue

The leaching residue of the cathode active material pyrolyzed at 500 °C was analysed using XRD and AAS, from both sulfuric acid and sodium hydroxide leaching media. The XRD results are shown in Figure 7. Most of the cathode active material dissolved in the leaching media, as indicated by the absence of LiFePO_4 peaks in the XRD patterns of both leaching media. Graphite peaks were present in the XRD analysis of the leaching residues, indicating that graphite did not dissolve in either sulfuric acid or sodium hydroxide. For sulfuric acid leaching residues, the peaks of C and Al_2O_3 were observed. Al_2O_3 likely originated from minor contaminants attached to the aluminium foil, which are stable and insoluble in acid due to their high Gibbs free energy [13]. C was the dominant phase in the sulfuric acid leaching residues, suggesting that most of the metal elements were dissolved, while graphite remained as the main component of the residue. In sodium hydroxide leaching residues, C and Fe_3O_4 peaks appeared, with undissolved iron remaining as Fe_3O_4 . This is supported by the research of Yang et al. [12], who reported that Fe_3O_4 was the dominant phase formed due to the oxidation of Fe^{2+} to Fe^{3+} by OH^- ions from NaOH.

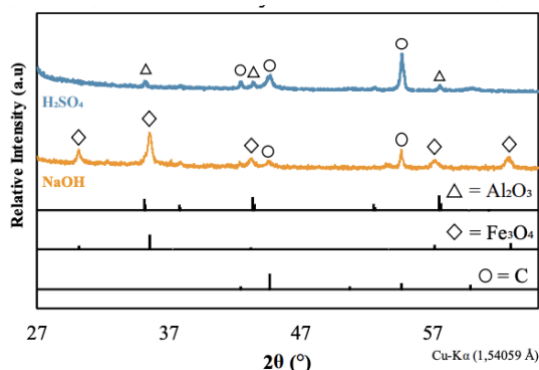


Fig. 7. XRD analysis of leaching residue of electrode active material pyrolyzed at 500 °C

Figure 8 and Figure 9 show the estimated composition of key elements (Li, Fe, Cu, and Al) in the leaching residue using sulfuric acid and sodium hydroxide as leaching media. Based on AAS analysis, lithium was still present in the leaching residue, even though lithium-containing phases were not detected in the XRD analysis. This is likely because the lithium phase is amorphous and thus undetectable by XRD. The leaching residue using sulfuric acid was dominated by lithium, while the residue from sodium hydroxide leaching was mainly composed of Fe.

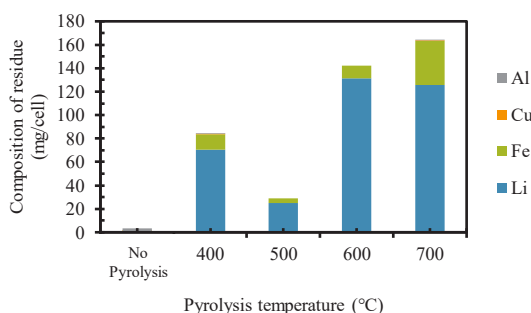


Fig. 8. Main element composition in the leaching residue with 2.5 M sulfuric acid as leaching media

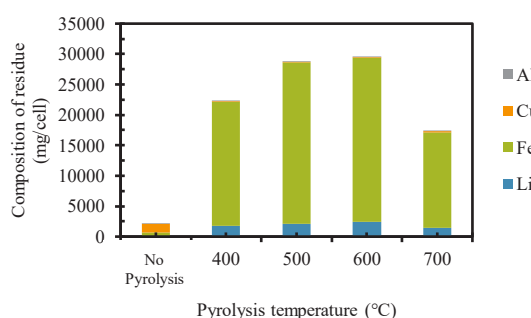


Fig. 9. Main element composition in the leaching residue with 5 M sodium hydroxide as leaching media

4 Conclusions

Based on the series of experiments conducted, the following conclusions can be drawn:

1. The highest recovery of -45 mesh electrode active material per battery cell was obtained at a pyrolysis

temperature of 600 °C, with a mass 0.5 g higher than that obtained at 500 °C. However, the highest Li concentration was found in the -45 mesh material after pyrolysis at 500 °C. No phase transformation of LiFePO₄ or metallic formation was observed at any tested pyrolysis temperature.

2. The highest Li concentration in the leachate was achieved from the leaching of electrode active material pyrolysed at 500 °C, when leached with either sulfuric acid or sodium hydroxide, indicating that pyrolysis at 500 °C provides optimal conditions for Li recovery from spent LFP batteries
3. Li leaching with sulfuric acid produced higher dissolved Li concentrations compared to sodium hydroxide across all pyrolysis temperature variations. On the other hand, sodium hydroxide leaching showed better selectivity in separating lithium and other metals from Fe, with Fe extraction percentages in the leachate consistently approaching zero for all tested pyrolysis temperatures.

References

1. International Energy Agency, “Global Energy Review 2025”. [Online]. Available: www.iea.org
2. International Energy Agency, “Net Zero by 2050 - A Roadmap for the Global Energy Sector”, 2050. [Online]. Available: www.iea.org.
3. K. Knehr, J. Kubal, P. A. Nelson, and S. Ahmed, *Cost Analysis and Projections for U.S.-Manufactured Automotive Lithium-ion Batteries*, Final Report, Argonne National Laboratory, 2024. ANL/CSE-24/1. [Online]. Available: www.anl.gov.
4. W. Fu, Y. Wang, K. Kong, D. Kim, F. Wang, and G. Yushin, “Materials and processing of lithium-ion battery cathodes,” *Nanoenergy Adv.*, **3**, pp. 138-154, 2023, doi: 10.3390/nanoenergyadv3020008.
5. A. K. Koech, G. Mwandila, F. Mulolani, and P. Mwaanga, “Lithium-ion battery fundamentals and exploration of cathode materials: A review,” *South African Journal of Chemical Engineering*, **50**, pp. 321-339, 2024, doi: 10.1016/j.sajce.2024.09.008.
6. Y. Lu and T. Zhu, “Status and prospects of lithium iron phosphate manufacturing in the lithium battery industry”, *MRS Communications*, **14**, no. 5, pp. 888-899, 2024, doi: 10.1557/s43579-024-00644-2.
7. T. Zhao, W. Li, M. Traversy, Y. Choi, A. Ghahreman, Z. Zhao, C. Zhang, W. Zhao, and Y. Song, “A review on the recycling of spent lithium iron phosphate batteries,” *Journal of Environmental Management*, **351**, p. 119670, 2024. doi: 10.1016/j.jenvman.2023.119670.
8. D. d. S. Vasconcelos, J. A. S. Tenório, A. B. Botelho Junior, and D. C. R. Espinosa, “Circular recycling strategies for LFP batteries: A review focusing on hydrometallurgy sustainable

- processing,” *Metals*, **13**, no. 3, p. 543, 2023, doi: 10.3390/met13030543.
9. G. P. Laksono, “Studi Variasi Jalur *Pre-treatment* dalam Proses Daur Ulang Baterai Litium Besi Fosfat,” Institut Teknologi Bandung, 2025.
 10. F. Diaz, Y. Wang, R. Weyhe, dan B. Friedrich, “Gas generation measurement and evaluation during mechanical processing and thermal treatment of spent Li-ion batteries,” *Waste Management*, **84**, pp. 102–111, 2019, doi: 10.1016/j.wasman.2018.11.029.
 11. Y. Jie, S. Yang, Y. Li, F. Hu, D. Zhao, D. Chang, Y. Lai, dan Y. Chen, “Waste organic compounds thermal treatment and valuable cathode materials recovery from spent LiFePO₄ batteries by vacuum pyrolysis,” *ACS Sustainable Chemistry & Engineering*, **8**, pp. 4814–4823, 2020, doi: 10.1021/acssuschemeng.0c07424.
 12. W. Yang, X. Liu, X. Zhou, J. Tang, F. Su, Z. Li, J. Yang, dan Y. Ma, “Mechanism of selective lithium extraction from spent LiFePO₄ cathodes in oxidizing alkaline leaching system,” *Separation and Purification Technology*, **329**, p. 125237, 2024, doi: 10.1016/j.seppur.2023.125237.
 13. M. Lin, J. Zhang, C. Xu, Y. Chen, dan C. Wang, “Two targets, one strike: Efficient recovery of lithium and simultaneous removal of impurities from spent LFP batteries via ferric ions-assisted air oxidation method,” *Separation and Purification Technology*, **355**, p. 129558, 2025, doi: 10.1016/j.seppur.2024.129558.